563580

Twenty-Eighth Symposium (International) on Combustion/The Combustion Institute, 2000/pp. 000–000

EFFECTS OF INERT DUST CLOUDS ON THE EXTINCTION OF STRAINED, LAMINAR FLAMES AT NORMAL AND MICRO GRAVITY

M. GURHAN ANDAC, FOKION N. EGOLFOPOULOS, CHARLES S. CAMPBELL AND ROMAIN LAUVERGNE

Department of Aerospace and Mechanical Engineering
University of Southern California
Los Angeles, CA, 90089-1453, USA

A combined experimental and detailed numerical study was conducted on the interaction between chemically inert solid particles and strained, atmospheric methane/air and propane/air laminar flames, both premixed and non-premixed. Experimentally, the opposed jet configuration was used with the addition of a particle seeder capable of operating in conditions of varying gravity. The particle seeding system was calibrated under both normal and micro gravity, and a noticeable gravitational effect was observed. Flame extinction experiments were conducted at normal gravity by seeding inert particles at various number densities and sizes into the reacting gas phase. Experimental data were taken for 20 and 37 μ nickel alloy and 25 and 60 μ aluminum oxide particles. The experiments were simulated by solving along the stagnation streamline the conservation equations of mass, momentum, energy, and species conservation for both phases, with detailed descriptions of chemical kinetics, molecular transport, and thermal radiation. The experimental data were compared with numerical simulations, and insight was provided into the effects on extinction of the fuel type, equivalence ratio, flame configuration, strain rate, particle type, particle size, particle mass delivery rate, the orientation of particle injection with respect to the flame, and gravity. It was found that for the same injected solid mass, larger particles can result in more effective flame cooling compared to smaller particles, despite the fact that equivalent masses of the larger particles have smaller total surface area to volume ratio. This counterintuitive finding resulted from the fact that the heat exchange between the two phases is controlled by the synergistic effect of the total contact area and the temperature difference between the two phases. Results also demonstrate that meaningful scaling of interactions between the two phases may not be possible due to the complexity of the couplings between the dynamic and thermal parameters of the problem.

Introduction

The physical mechanisms of two-phase reacting flows are poorly understood compared to those of pure gaseous flows. While substantial amount of work has been devoted to sprays, less attention has been given to the details of reacting dusty flows. Even chemically inert particles can alter the flammability and extinction limits of combustible mixtures through strong dynamic and thermal couplings. The presence of Stokes drag, phoretic, and gravitational forces on the particles affect the dynamic interaction between the phases. Also, as the solid phase possesses larger thermal inertia relative to the gas, substantial temperature differences between the two phases can develop.

The stagnation flow configuration has been used in the past for the study of spray and particle flows, as it offers advantages both in experimentation and modeling [1–5]. Numerically, the need for a hybrid Eulerian–Lagrangian approach has been identified by Continillo and Sirignano [1] and has allowed for the prediction of the phenomenon of droplet flow reversal [2,3], which has been observed experimentally [3]. Gomez and Rosner [4] have conducted a detailed study on the particle response in opposed-jet configurations to determine thermophoretic diffusivities. Sung et al. [5] have numerically studied dusty flows in opposed-jet configurations, with emphasis on the dynamic coupling. An extensive list of pertinent studies can be found in Ref. [6]. In previous studies on dusty flows [4,5], the thermal coupling between the two phases as well as the effects of particle mass delivery rate and gravity were not considered. In Ref. [6] such effects were partially addressed for premixed flames through detailed numerical simulations of the two-phase stagnation flow configuration.

The objective of the present work was to conduct a combined experimental and detailed numerical simulation in order to assess the role of inert particles on flame extinction. The results were used to derive physical insight into the mechanisms that control the dynamic and thermal interactions between the two phases. Gravity was included as a parameter, as its effects can be quite complex.

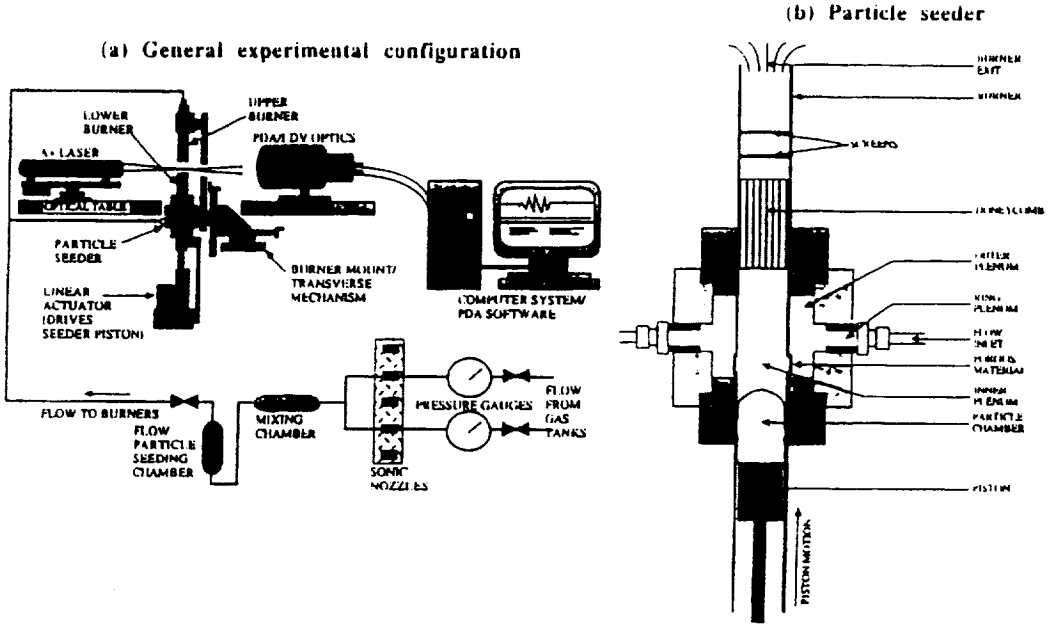

FIG. 1. (a) General experimental configuration. (b) Schematic of the particle seeder.

Experimental Approach

The experimental configuration, shown in Fig. 1a, includes the use of two counterflowing jets exiting from two opposing 22 mm diameter burners separated by a 14 mm distance. Fig. 1b depicts a schematic of the particle seeder, which utilizes a piston feeder as proposed in Ref. [7]. Attached beneath the bottom burner is a piston that feeds the particles into the flow at a constant rate. Chemically inert aluminum oxide and nickel alloy particles were used (these flames are too cool for nickel ignition). Particle sizes were determined to be within 2–5 μ of the nominal size for 90% of the particles. The particle mass delivery is determined by both the piston speed and the flow rate. The gas flow enters the top of the piston shaft through sixteen 1 mm diameter holes equally spaced around the shaft, which locally increase the gas velocity and improve the entrainment of particles into the flow. This design allows for seeding under both normal (1 g) and micro gravity (μg). However, it should be obvious that the particle pickup is strongly affected by gravitational forces. The particle seeder was calibrated by seeding the particles into the air flow for a specified time and their subsequent collection in ultralight bags at the burner exit. The delivered mass of the particles was determined by measuring the mass of the bag before and after the experiment by using a high-precision scale. Calibration in μg was performed on board NASA's KC-135 plane.

Premixed and non-premixed flame extinction experiments were conducted in 1 g by varying the particle type, size, and mass delivery rate as well as the gas phase equivalence ratio, fuel type, flame configuration, and strain rate. In all these experiments, the particles were seeded from the lower burner.

Two types of premixed flame configurations were studied. The first included the use of the symmetric twin-flame that results by impinging on each other two fuel/air jets of identical composition. For this configuration, the particles preferentially cool the first flame that they encounter and may or may not have a chance to directly cool the second flame, depending both on the ability of the particles to penetrate the gas-phase stagnation plane (GSP) and on the particle's thermal state as they reach the second flame. The second configuration used is a single flame that results by impinging a fuel/air jet on an opposing air jet. Given that the particles are seeded from the lower burner, the extinction of single flames was studied by stabilizing them on both sides of the GSP. If the single flame is stabilized below the GSP, then it is directly cooled by the particles. If the single flame is stabilized above the GSP, only large particles would possess the inertia to cross the stagnation plane and directly affect the flame.

In the non-premixed flame experiments, a mixture of fuel and nitrogen gas was supplied from the bottom burner, while the air jet was supplied from the upper burner.

For all cases, the flames would be first established at conditions close to the extinction state. Then, the

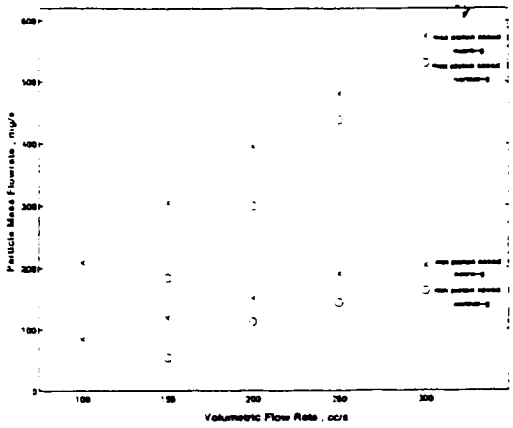

FIG. 2. Particle seeder calibration curves for 25.0 μ aluminum oxide particles in normal and micro gravity.

local strain rate, based on the maximum velocity gradient in the hydrodynamic zone, was measured by using laser Doppler velocimetry (LDV). Subsequently, the piston seeder was turned on, feeding the particles at a constant rate. The fuel flow rate was then decreased very slowly, until the flames were extinguished due to the synergistic effect of the strain rate and the heat loss to the particles. In order to isolate the effect of particle size on flame cooling, the piston speeds were set to deliver equal amounts of mass of different size particles. The accuracy of the data is limited by the accuracy of calibration of the sonic nozzles, which is 0.5%, and the accuracy of LDV, which is 1 cm/s. The accuracy of calibrating the particle mass flow rate was found to be less than 10%.

Numerical Approach

A set of equations along the system centerline has been developed for both phases [6]. A quasi one-dimensional set of equations was derived for the gas phase along the stagnation streamline, similar to those in Ref. [8]. The particle equations were formulated for each particle independently, valid for small particle number densities.

For inert particles, the gas phase continuity and species equations are identical to those of Ref. [8]. The gas-phase momentum equation, however, was modified by adding a term representing the force exerted by the particles on the gas. The gas-phase energy equation was also modified by including terms describing the conductive/convective/radiative heat exchange between the two phases. The axial particle momentum equation includes the Stokes drag, thermophoretic, and gravitational forces; the system configuration is assumed to be vertical so that gravity acts in the axial direction. The particle energy equation includes the contributions of conductive/convective heat exchange between the two phases and the radiative energy exchange between the particles and the surrounding gas. Finally, a conservation equation is used to determine the particle number density.

The solution was obtained by simultaneously integrating the entire system of equations for both phases. For the integration of the gas-phase equations, a Eulerian frame of reference was used, while the particle equations were integrated in a Lagrangian frame of reference in order to properly describe particle reversal [1,6]. Detailed kinetics [9] were used, and the code was integrated with the CHEMKIN [10] and TRANSPORT [11] subroutine packages.

Special care had to be taken in regions of particle reversal, as particle number density is singular (although integrable) at the points of reversal [6]. In the vicinity of particle stagnation plane (PSP), the particle velocities are small so that at equal time steps, the Lagrangian spatial resolution is substantially greater than the Eulerian one. Thus, convergence may not be possible if singular values of particle number densities are mapped from the Lagrangian grid onto a more coarsely resolved Eulerian grid, causing discontinuities in property values and thus in the phase interaction terms of the gas-phase momentum and energy equations. It was found that this problem can be resolved if the Eulerian grid is finely resolved around PSPs.

Results and Discussion

au: see query #1

Experimental Results

Flame extinction experiments were conducted on the extinction of methane and propane flames for the following four cases:

1. Premixed, symmetric across the GSP twin-flames
2. Premixed, single-flame stabilized below the GSP
3. Premixed, single-flame stabilized above the GSP
4. Non-premixed flames stabilized below the GSP

In order to determine the particle mass delivery, the seeder had to be calibrated for all particle types and sizes. An example of the calibrations is shown in Fig. 2 for 25 μ aluminum oxide particles. It can be seen that the particle mass flow rate increases linearly with both gas flow rate and with the piston speed. Comparisons between the calibration curves at 1 g and μg reveal that for a given piston speed and gas flowrate, the particle mass flowrate at μg is consistently higher as no gravitational forces oppose the particle motion. For the same reasons, calibration below 150 cm^3/s flow rate was not possible in 1 g, although easily achieved in μg.

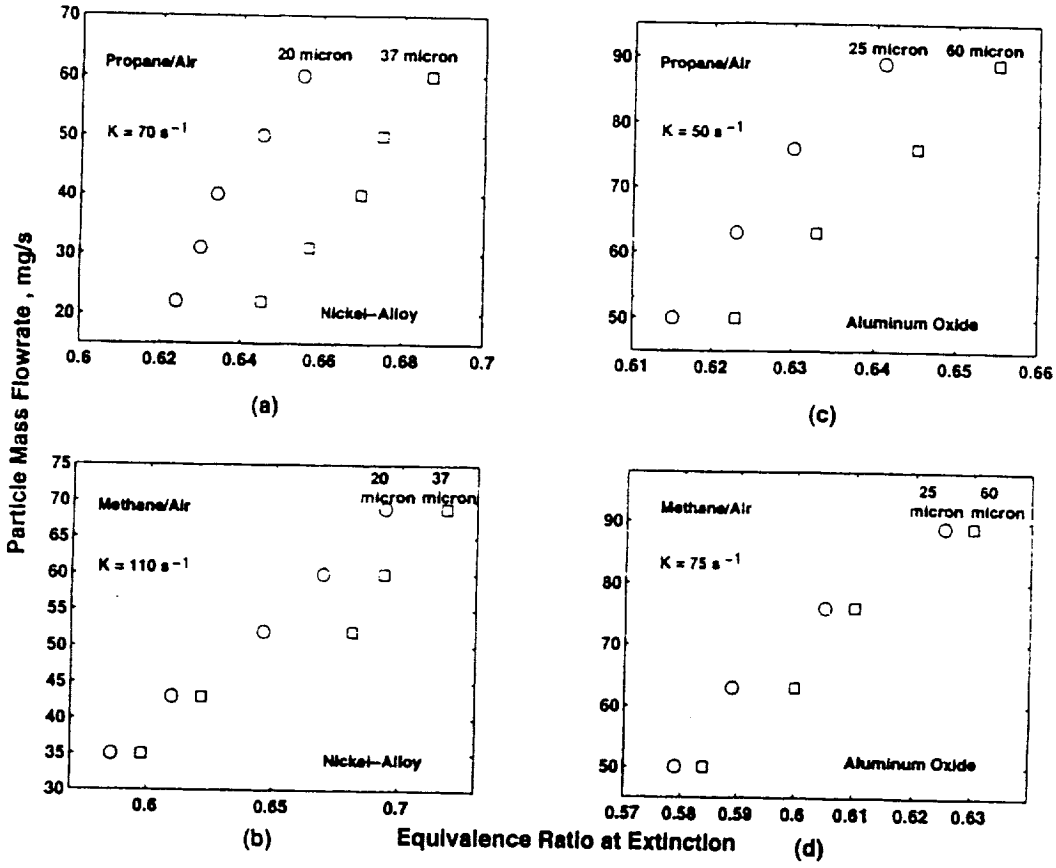

FIG. 3. Experimental data on twin premixed flame extinction. Injection velocities at nozzle exits: (a) 46.4 cm/s, (b) 53.4 cm/s, (c) and (d) 33.5 cm/s.

Flame extinction experiments performed in 1 g can be seen in Fig. 3, which depicts comparisons of the cooling effects of 20 and 37 μ nickel alloy and 25 and 60 μ aluminum oxide particles on lean premixed propane/air and methane/air twin flames. All flames shown in each frame experience the same strain rate. Note that in all cases, the data for the larger particles fall below those for the smaller particles, indicating that for the same particle mass delivery rate, larger particles extinguish stronger flames. This result is counterintuitive, as for the same particle mass the smaller particles expose more surface area to the gas phase, which should allow more efficient heat transfer.

The results of Fig. 3 also reveal that for the same conditions, the extinction equivalence ratios are higher for propane flames, as their $Le > 1$ so that their extinction is more susceptible to strain rate and heat losses. It was also found that for the same conditions, the nickel alloy particles extinguish stronger flames compared to aluminum oxide. This may be explained by a combination of two effects. First of all, nickel alloy particles have about twice the specific heat of aluminum oxide. Second, the nickel alloy particles are nearly spherical, while the aluminum oxide are quite angular. As a result, the aluminum oxide particles have a larger surface-area-to-volume ratio, much like smaller spherical particles.

Figure 4a depicts a comparison of flame extinction results obtained for the case of single methane/air premixed flames stabilized below the GSP and twin methane/air premixed flames. Comparisons of single methane/air flames stabilized below and above GSP are shown in Fig. 4b. Recall that particles are injected from the bottom burner in all cases. Noticeably, stronger flames are extinguished in the bottom flame configuration compared to the twin flame case with almost the same strain rate and particle mass delivery rate. This is physically reasonable, as twin flames are adiabatic, while single flames suffer from heat losses to air stream. The results of Fig. 4b indicate that the particles are able to extinguish stronger flames in the bottom flame configuration

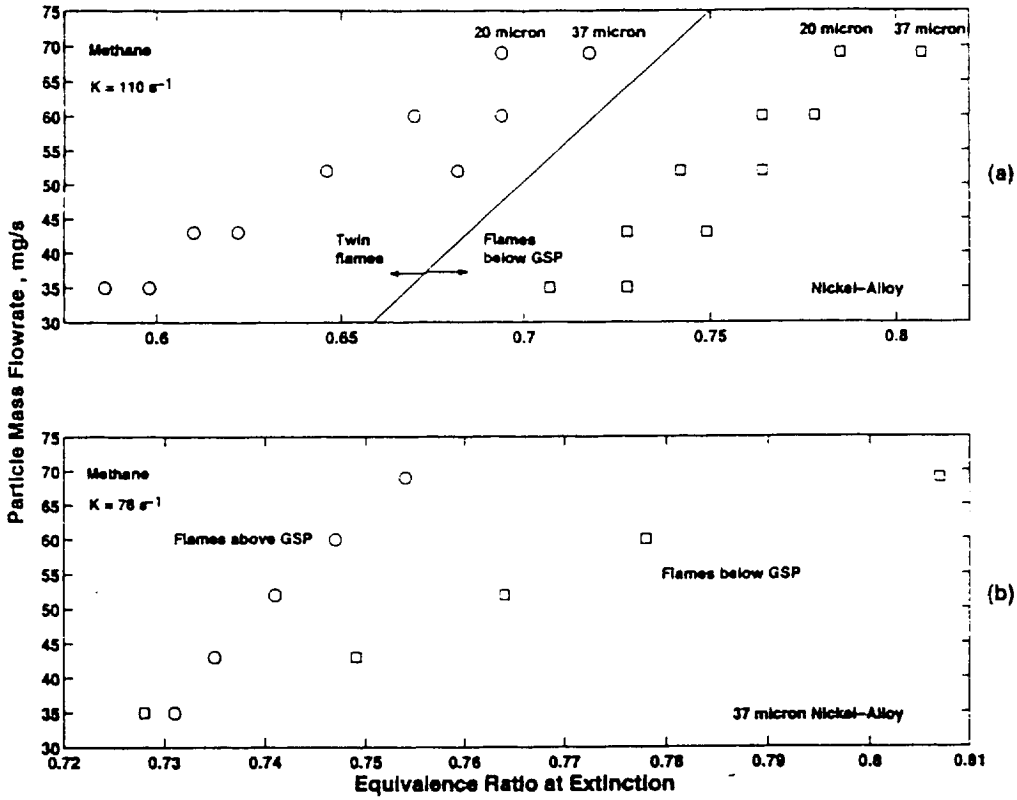

FIG. 4. Experimental data on extinction of (a) twin and single flames stabilized above GSP and (b) single flames stabilized below and above GSP. Injection velocities at nozzle exits 53.4 cm/s.

compared to the top flame configuration. In the bottom (single) flame configuration, particles reach the flame region with temperatures nearly equal to the ambient temperature at which they were injected. However, in the top (single) flame configuration, particles cross the stagnation plane and travel through the region of hot combustion products, the downstream of the top flame. As they move against an opposing flow, their velocities are also reduced and their residence times within the hot product increases. Thus, their temperatures are raised close to the flame temperature by the time they reach the reaction zone of the top flame. As a result, the particles cannot effectively cool the top flame, and only relatively weak flames can be extinguished.

Figure 5 depicts results of non-premixed flame extinction. Fuel/nitrogen mixtures were supplied from the bottom burner and air was supplied from the top burner. For these reactant concentrations, the flames were stabilized below the GSP, that is, on the particle injection side. Again, stronger flames are extinguished by the larger particles in all cases.

Numerical Results

Numerical simulations were conducted by injecting 25 and 60 μ aluminum oxide particles into twin flame methane/air flames. It was observed that, as in the experiments, 60 μ particles cool the flames more effectively than the 25 μ particles.

In order to understand this behavior, the detailed flame structure was analyzed. Figure 6a depicts the spatial variation of the gas and particle phase temperatures obtained for both cases; in this and all following figures, the particles are injected from the left boundary, which corresponds to the lower burner.

Note that there are two mechanisms that affect the heat transfer between the two phases. The first is the total particle surface area available for heat transfer, and the second is the temperature difference between the two phases. For the same mass of particles delivered, small particles possess larger total surface area. Thus, from this respect, the total area mechanism favors the small particles. However, because of their thermal inertia, large particles develop larger temperature differences with the gas phase. Thus, the temperature difference mechanism favors the large particles. It is the competition between these two factors that determines which size cools more effectively.

Figure 6b depicts the spatial variation of the heat transfer between the two phases for the two cases

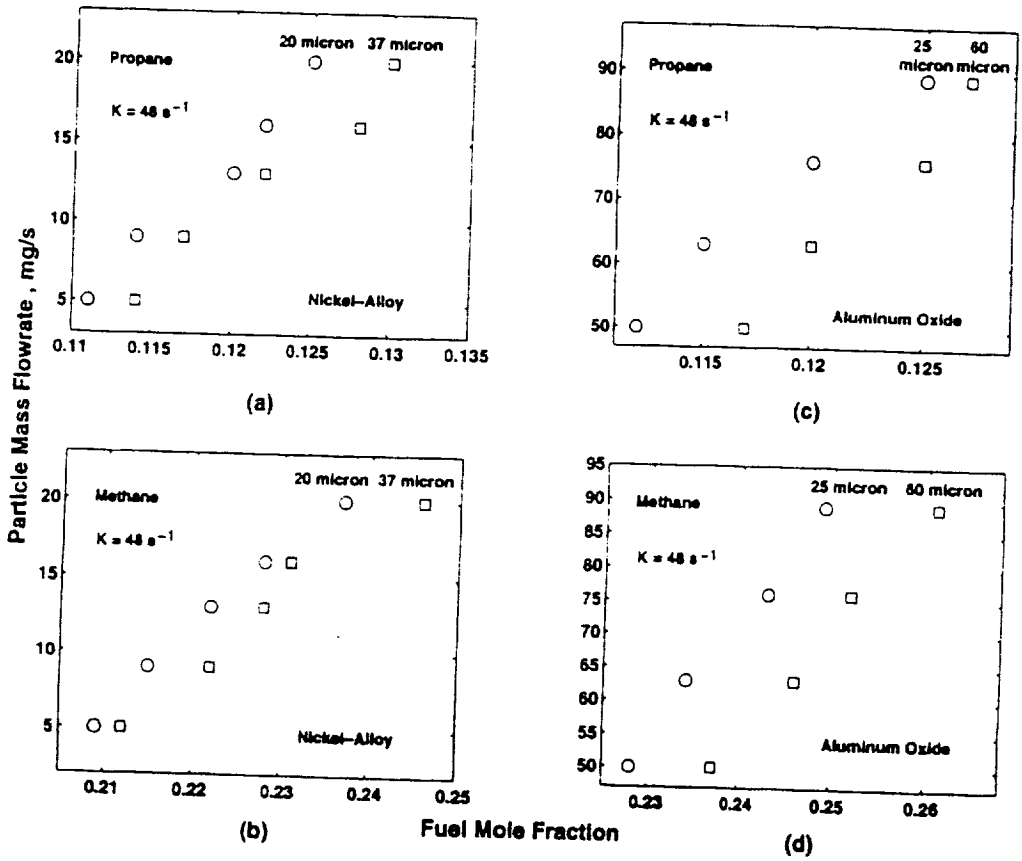

FIG. 5. Experimental data on non-premixed flame extinction, with injection velocities at nozzle exits 33.5 cm/s.

being considered. It can be seen that 25 μ particles remove more heat from the flames in the preheat region, and their temperature closely follows the gas phase (Fig. 6a). However, the 60 μ particles stay relatively cool until they reach deeper into the flame, resulting in increased heat loss within the reaction zone. Note that in the reaction zone of the bottom flame, the temperature difference between the two phases for the 60 μ case is of the order of the ratio of the total surface areas of the two sizes. Thus, the temperature difference factor dominates the area factor within the reaction zone, demonstrating why large particles can extinguish stronger flames.

Figure 7 depicts additional numerical results, which reveal that the physics can be even more complex. Here, the variation of the maximum flame temperature with the strain rate is shown for methane/air premixed flames at an equivalence ratio of 0.648 seeded by 20 and 37 μ nickel alloy particles. In both cases, the delivered particle mass density is 0.065 mg/cm^3. Note that the large particles yield larger reductions in the gas-phase temperature up to a certain strain rate (here about 140 s^{-1}). Beyond this strain rate value, smaller particles exhibit a better cooling efficiency. (It should be noted that all of the experiments presented above were below this critical strain rate.) This is easily understood as, at high strain rates, the large inertia of the large particles rapidly transports them through the flame, leaving little time to remove much heat from the flames. On the other hand, small particles have less inertia as they approach the stagnation plane and reside longer within and thus can effectively cool the flame.

A quite complicated effect of both gravity and the particle mass delivery rate was found. Fig. 8 depicts the spatial variation of the gas and particles velocities for a methane/air flame with equivalence ratio of 0.584 seeded by 60 μ aluminum oxide particles, at 0 g and 1 g, and for two different mass delivery rates, that is, 0.55 and 34.44 mg/s. In the 0 g case, particles penetrate deeper into the upper jet since gravity does not reduce their velocities as they approach the GSP. Fig. 8a and b depict the cases with 0.58 mg/s mass delivery rate. In both cases, particles undergo reversals and finally reach equilibrium at the stagnation plane for the 0 g case (Fig. 8a) and at a lower elevation, where Stokes drag balances the gravitational force, for the 1 g case (Fig. 8b). Fig. 8c and d

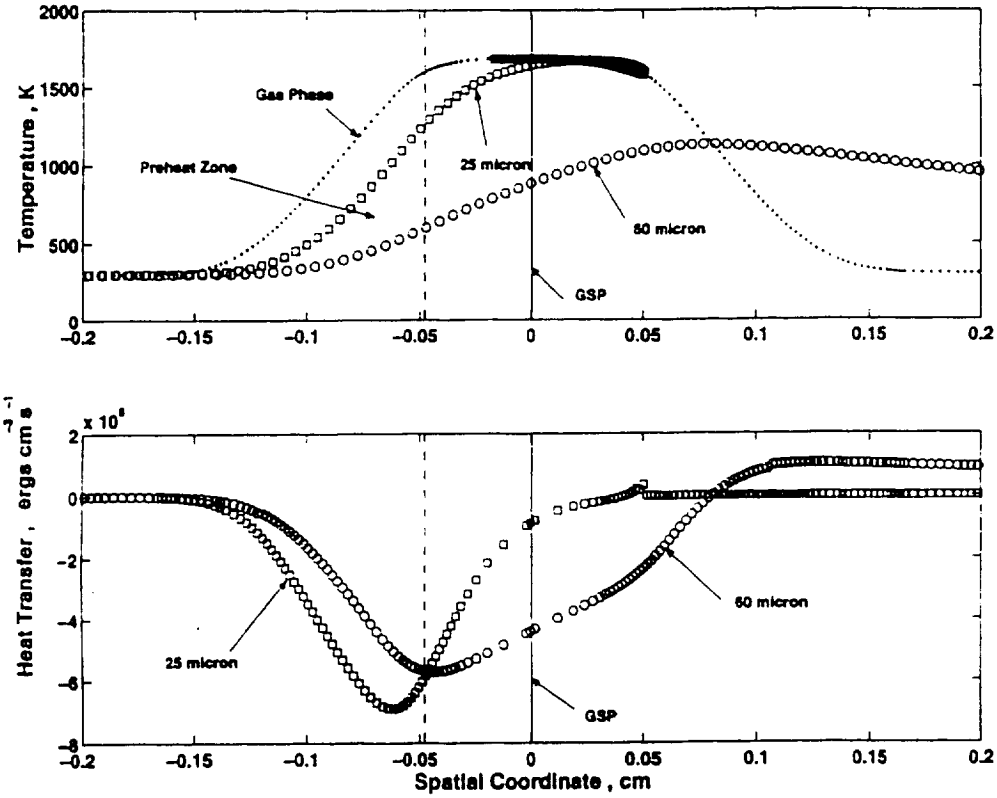

FIG. 6. Numerically determined (a) spatial variation of the gas and particle phase temperatures and (b) interphasial heat transfer, for twin, premixed methane/air flames with an equivalence ratio of 0.6, seeded with 25 and 60 μ aluminum oxide particles.

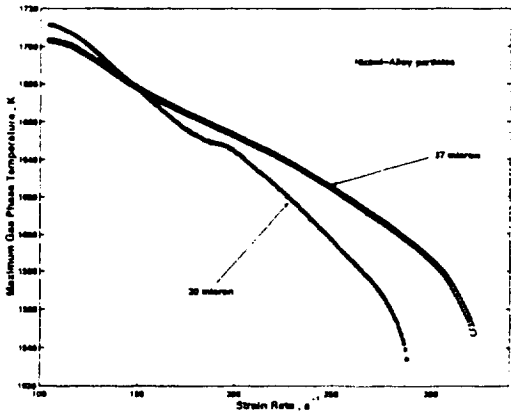

FIG. 7. Variation of numerically determined maximum gas-phase temperature with strain rate for twin, premixed methane/air flames with an equivalence ratio of 0.648, seeded with 20 and 37 μ nickel-alloy particles. Particle mass density ($n_p * m_p$, where m_p is a single particle mass) delivered at the exit is 0.065 mg/cm^3.

depict both results for mass delivery rate of 34.44 mg/s. In the 0 g case, however, particles behave much as in the lower mass delivery rate case. Notice, however, the significant mass delivery rate effect between the two 1 g cases, as shown in Fig. 8b and d. In the first case (Fig. 8b), the mass delivery rate is so small that has minimal effect on the particle trajectories. But in Fig. 8d, the mass delivery rate is large enough to remove significant amounts of energy from the lower flame. Thus, the thermal expansion and the resulting gas velocities are so small that Stokes drag cannot overcome gravity, and the particles fall back into the bottom nozzle.

These results demonstrate that the effects of particle injection are very complex, so complex as to suggest that any simple scaling of the problem may be all but impossible. For example, one might be tempted to suggest a scaling centering on a Stokes number based on the injection velocity (perhaps with the addition of a Froude number to capture the gravity effects). However, such a scaling misses a myriad of effects due to the strong coupling between the particle velocities and the thermal effects. For

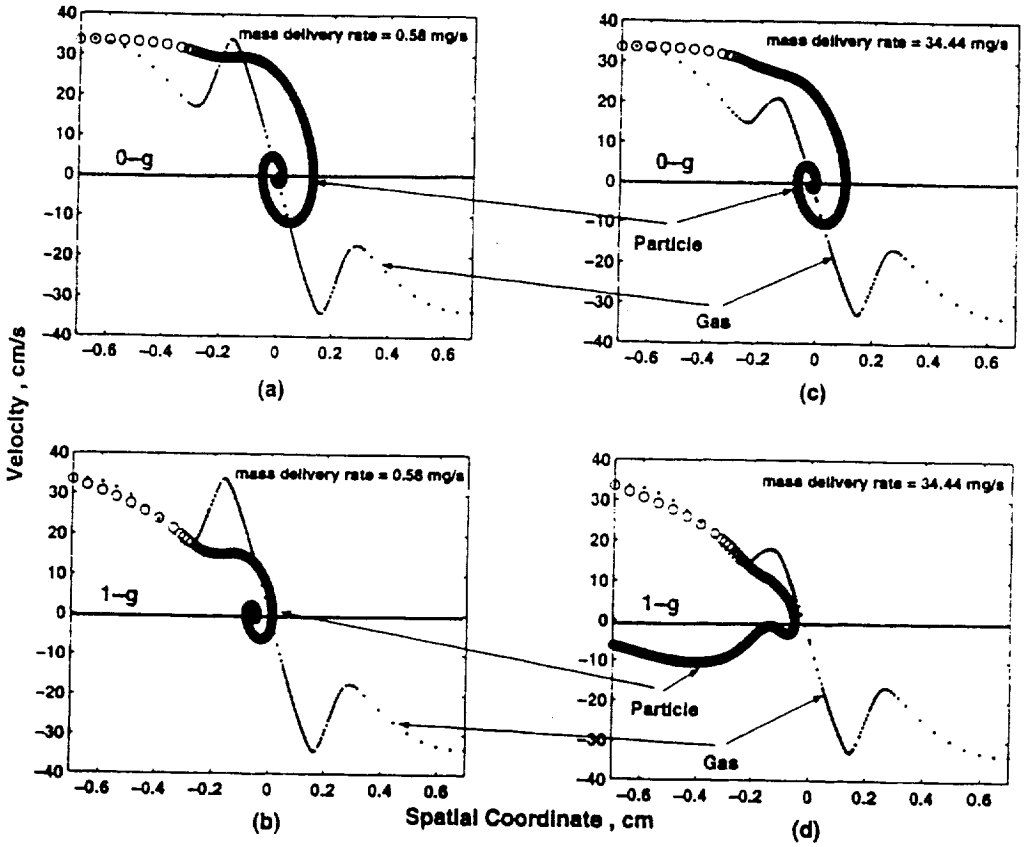

FIG. 8. Numerically determined spatial variations of gas and particle phase velocities for twin, premixed methane/air flames with an equivalence ratio of 0.584, seeded with 60 μ aluminum oxide, under conditions of (a) 0 g and mass delivery rate = 0.58 mg/s, (b) 1 g and mass delivery rate = 0.58 mg/s, (c) 0 g and mass delivery rate = 34.44 mg/s, and (d) 1 g and mass delivery rate = 34.44 mg/s.

example, as it is based on the injection velocities, such a scaling does not account for the presence or absence of particle reversals that are strongly affected by the gas accelerations in the flame expansion zones. This can be clearly seen by comparing Fig. 8b and d, which show that the smaller gas acceleration near a weaker flame can cause particles to fall back into the burner (Fig. 8d) rather than undergo a series of reversals (Fig. 8b). (Also, for the same reasons, the gravity effect on the location of the reversal would not be captured by a Froude number.) To describe these effects, one would also have to include thermal parameters, reflecting the strong effect of cooling on the Arrhenius behavior of the chemical kinetics (which cannot be scaled due to its nonlinear dependence on the temperature). One would be tempted to scale the particle mass delivery rate (apparent in Fig. 8) with the particle volume, but such a scaling would not reflect the particle size effects apparent in Figs. 3–7, as it is possible to have the same solid-phase concentration for a variety of sizes. For that matter, there does not appear to be a convenient length scale with which the diameter could be scaled that would properly reflect the effects of diameter on flame cooling. Consequently, no dimensional scaling of the problem makes itself apparent, and if possible would include a very large number of parameters that it could be scarcely said to simplify the problem.

Concluding Remarks

The effect of inert particle clouds on the extinction of strained premixed and non-premixed flames was studied experimentally and numerically in the counterflow configuration. The effects of fuel type, equivalence ratio, flame configuration, strain rate, particle type, size, delivery rate, injection orientation, and gravity were independently considered.

The experimental results revealed the surprising observation that large particles can cause more effective flame cooling compared to smaller particles.

The numerical simulations reproduced this behavior and showed that while similar masses of small particles possess more total surface area, the large particles can establish large temperature differences with the gas phase within the reaction zone and, thus, more effectively cool the flame. At high strain rates, however, the opposite trend was observed as large particles are quickly transported through the flame. The effect of gravity was found to be quite involved, coupling the strain rate, the flame temperature, and the particle mass delivery rate.

Finally, the complex coupling between the various parameters is so complex that meaningful scaling capturing all pertinent physics is not possible. Thus, caution is recommended in using traditional scaling arguments to describe phenomena related to reacting dusty flows.

Acknowledgments

This work was supported by NASA, grant no. NAG3-1577. The technical supervision of Dr. Ming-Shin Wu of the NASA Glenn Research Center is greatly appreciated.

REFERENCES

1. Continillo, G., and Sirignnano, W. A., *Combust. Flame* 81:325–340 (1990).
2. Chen, N. H., Rogg, B., and Bray, K. N. C., *Proc. Combust. Inst.* 24:1513–1521 (1992).
3. Chen, G., and Gomez, A., *Proc. Combust. Inst.* 24:1531–1539 (1992).
4. Gomez, A., and Rosner, D. E., *Combust. Sci. Technol.* 89:335–362 (1993).
5. Sung, C. J., Law, C. K., and Axelbaum, R. L., *Combust. Sci. Technol.* 99:119–132 (1994).
6. Egolfopoulos, F. N., and Campbell, C. S., *Combust. Flame* 117:206–226 (1999).
7. Goroshin, S., Kleine, H., Lee, J. H. S., and Frost, D., "Microgravity Combustion of Dust Clouds: Quenching Distance Measurements," Third International Microgravity Combustion Symposium, NASA Lewis Research Center, Cleveland, Ohio, April, 1995.
8. Kee, R. J., Miller, J. A., Evans, G. H., and Dixon-Lewis, G., *Proc. Combust. Inst.* 22:1479–1494 (1988).
9. Bowman, C. T., Frenklach, M., Gardiner, W. R., and Smith, G., *The GRI 3.0 Chemical Kinetic Mechanism*, http://www.me.berkeley.edu/gri_mech/, 1999.
10. Kee, R. J., Warnatz, J., and Miller, J. A., Sandia report SAND83-8209.
11. Kee, R. J., Rupley, F. M., and Miller, J. A., Sandia report SAND89-8009.